Climate Dynamics (2020) 54:1367–1382
https://doi.org/10.1007/s00382-019-05063-x

Eastern Mediterranean summer temperatures since 730 CE from Mt. Smolikas tree-ring densities

Jan Esper[1] · Lara Klippel[1] · Paul J. Krusic[2,3,4] · Oliver Konter[1] · Christoph C. Raible[5,6] · Elena Xoplaki[7] · Jürg Luterbacher[7,8] · Ulf Büntgen[2,9,10]

Received: 2 August 2019 / Accepted: 19 November 2019 / Published online: 23 November 2019

Abstract

The Mediterranean has been identified as particularly vulnerable to climate change, yet a high-resolution temperature reconstruction extending back into the Medieval Warm Period is still lacking. Here we present such a record from a high-elevation site on Mt. Smolikas in northern Greece, where some of Europe's oldest trees provide evidence of warm season temperature variability back to 730 CE. The reconstruction is derived from 192 annually resolved, latewood density series from ancient living and relict *Pinus heldreichii* trees calibrating at $r_{1911–2015} = 0.73$ against regional July–September (JAS) temperatures. Although the recent 1985–2014 period was the warmest 30-year interval (JAS $T_{wrt.1961–1990} = +0.71$ °C) since the eleventh century, temperatures during the ninth to tenth centuries were even warmer, including the warmest reconstructed 30-year period from 876–905 (+0.78 °C). These differences between warm periods are statistically insignificant though. Several distinct cold episodes punctuate the Little Ice Age, albeit the coldest 30-year period is centered during high medieval times from 997–1026 (−1.63 °C). Comparison with reconstructions from the Alps and Scandinavia shows that a similar cold episode occurred in central Europe but was absent at northern latitudes. The reconstructions also reveal different millennial-scale temperature trends (NEur = −0.73 °C/1000 years, CEur = −0.13 °C, SEur = +0.23 °C) potentially triggered by latitudinal changes in summer insolation due to orbital forcing. These features, the opposing millennial-scale temperature trends and the medieval multi-decadal cooling recorded in Central Europe and the Mediterranean, are not well captured in state-of-the-art climate model simulations.

Keywords Temperature reconstruction · *Pinus heldreichii* · Maximum latewood density · Medieval warm period · Orbital forcing · Greece

✉ Jan Esper
esper@uni-mainz.de

[1] Department of Geography, Johannes Gutenberg University, Mainz, Germany

[2] Department of Geography, University of Cambridge, Cambridge, UK

[3] Department of Physical Geography, Stockholm University, Stockholm, Sweden

[4] Navarino Environmental Observatory, Navarino Dunes, Messenia, Greece

[5] Physics Institute, University of Bern, Bern, Switzerland

[6] Oeschger Centre for Climate Change Research, Bern, Switzerland

[7] Department of Geography, Justus Liebig University, Giessen, Germany

[8] Centre of International Development and Environmental Research, Justus Liebig University, Giessen, Germany

[9] Swiss Federal Research Institute WSL, Birmensdorf, Switzerland

[10] Global Change Research Centre AS CR v.v.i., Brno, Czech Republic

1 Introduction

Several tree-ring chronologies derived from maximum latewood density (MXD) appear in the top group of globally ranked, annually resolved (Büntgen et al. 2018), millennial-length temperature reconstructions (Esper et al. 2016). Among the ten best-scoring records are the MXD-based N-Scan (rank #1; Esper et al. 2012) and Torneträsk (#9; Briffa et al. 1992; Grudd 2008; Melvin et al. 2013; Schweingruber et al. 1988) chronologies from Scandinavia, subsequently combined in a northern European composite (Esper et al. 2014), the Lötschental chronology from the Swiss Alps (#6; Büntgen et al. 2006), and a chronology from western Siberia pooling together MXD and tree-ring width (TRW) data from the Polar Ural and Yamal (#4; Briffa et al. 2013). Compared to the more widespread TRW based climate reconstructions, MXD records typically contain less biological memory (Esper et al. 2015a), calibrate better against instrumental temperatures (Briffa et al. 1998b), and provide superior estimates of high-to-low frequency warm season temperature variability (Schneider et al. 2015; Wilson et al. 2016). MXD chronologies are particularly strong in preserving the full spectrum of climate variability (Franke et al. 2013), from inter-annual to millennial scales, so that the reconstructions from this proxy can be used to evaluate the effects of volcanic (Briffa et al. 1998a), solar (Luckman and Wilson 2005), greenhouse gas (Büntgen et al. 2011), and even orbital forcing (Esper et al. 2012) on the climate system.

Temperature reconstructions extending back into the first millennium CE are critically important to evaluate the most recent, naturally forced, warm episode during high medieval times, the Medieval Warm Period from ~ 800–1200 CE (MWP, Lamb 1965; Esper and Frank 2009; Jones et al. 2009). In Europe, annually resolved temperatures during the MWP are robustly captured by two MXD-based reconstructions, the northern European composite (NEur hereafter; Esper et al. 2014), the world's longest such record, extending back to 218 BC, and the Swiss Alps record from central Europe (CEur hereafter; Büntgen et al. 2006) extending back to 755 CE. No such record has yet been developed from the Mediterranean region (Luterbacher et al. 2016). South of the Alps, the longest MXD-based temperature reconstruction is from a very old *Pinus uncinata* stand in the Spanish Pyrenees, however this chronology contains just a single tree in 1000 CE, thereby excluding assessments of the MWP in the western Mediterranean (Büntgen et al. 2008, 2017; Esper et al. 2015b). Other important, yet too short, records are a June–August temperature reconstruction from *Larix decidua* TRW in the Maritime French Alps, with just five trees in 1000 CE (Büntgen et al. 2012), and a similarly replicated January-May temperature reconstruction from *Juniperus excelsa* $\delta^{13}C$ data from the Turkish Taurus Mountains reaching back to 1125 CE (Heinrich et al. 2013). Other high-resolution records providing quantitative estimates of climate variability in the Mediterranean are derived from trees that are predominantly sensitive to hydroclimate variations. The longest of these include spring to summer drought reconstructions from TRW data of giant *Cedrus atlantica* in Morocco (Esper et al. 2007) and Algeria (Touchan et al. 2008, 2011) reaching back to the tenth century CE, a May–June TRW precipitation reconstruction back to the eleventh century from multiple oak species in the north Aegean (Griggs et al. 2007), a May–June precipitation reconstruction back to the eleventh century from *J. excelsa* TRW in Turkey (Touchan et al. 2007), and a June–August precipitation reconstruction back to the twelfth century from *Pinus nigra* TRW in Corsica (Szymczak et al. 2014). However, none of these high-resolution reconstructions from the Mediterranean have sufficient sample replication large enough to produce calibrated temperature estimates, in °C, beyond the MWP (overview in Luterbacher et al. 2012).

A notable exception is the *Pinus heldreichii* treeline ecotone at Mt. Smolikas in northern Greece where the oldest dendrochronologically dated tree in Europe was found (Konter et al. 2017), and where relict boles remained for centuries on the ground (Fig. 1). TRW measurements from ~ 400 of these living and relict Bosnian pines enabled the development of a continuous chronology reaching back to 575 CE (Klippel et al. 2018), making this the longest and (during the early centuries) best replicated such timeseries from an ecologically constrained site in the Mediterranean region. The TRW chronology has been used to reconstruct the high frequency (inter-annual) variability of the Standardized Precipitation Index (SPI, McKee et al. 1993) over the past 1286 years, and enabled the detection of 51 dry and 42 pluvial extreme events since early medieval times (Klippel et al. 2018). A previously published late summer temperature MXD reconstruction, based on a subset of 69 trees and reaching back to the early eighth century (Klippel et al. 2019a), had to be constrained to a description of inter-annual variability and extremes as more data were needed to adequately describe high-to-low frequency temperature variance beyond the past millennium (Briffa et al. 1992; Esper et al. 2003).

Here, we present this reconstruction, based on 192 *P. heldreichii* MXD measurement series, produced over the past 3 years using high-resolution radiodensitometry (Schweingruber et al. 1978). First, we introduce the tree-ring sampling site on Mt. Smolikas in northern Greece and the methods used to develop an MXD chronology preserving high-to-low frequency variance over the past 1300 years. We then detail how this record calibrates against regional

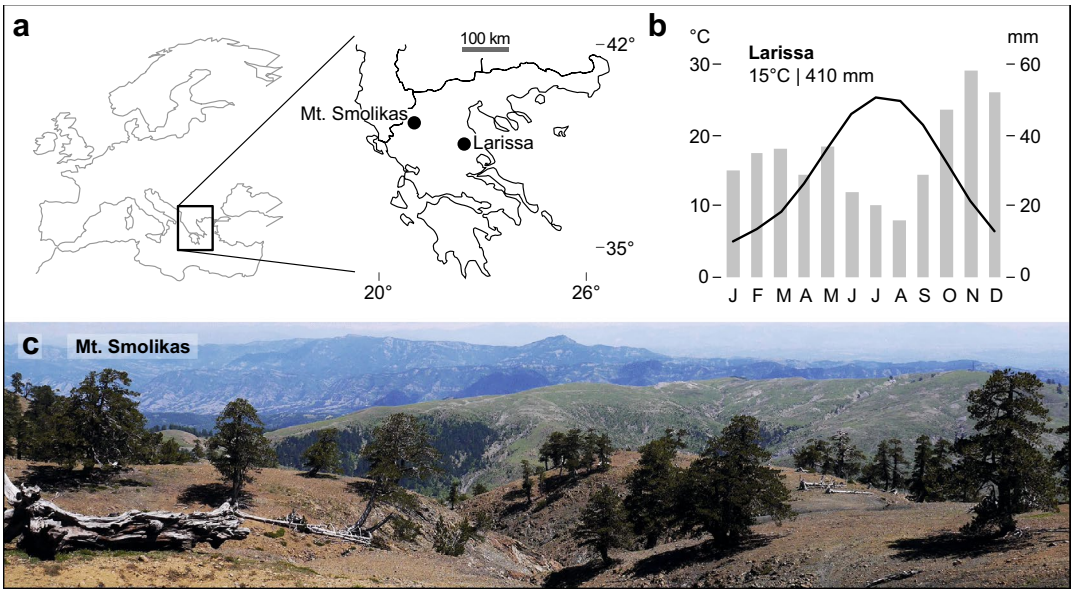

Fig. 1 Location of the Mt. Smolikas tree site and Larissa temperature station (**a**), the Larissa climate diagram (**b**), and a photograph of living and relict *P. heldreichii* in 2000–2200 m a.s.l. on Mt. Smolikas (**c**)

temperature data, and highlight the coldest and warmest reconstructed periods since early medieval times in the eastern Mediterranean basin. The reconstruction is compared with similar records from the Alps (CEur) and northern Scandinavia (NEur), with emphasis on retained millennial-scale temperature trends as well as the deviations during the putative MWP. These features, the lowest frequency trends and MWP temperature variability, are assessed using state-of-the-art climate model simulations to provide insight into some of the potential climate forcing factors driving Mediterranean and European climate dynamics.

2 Materials and methods

2.1 Mt. Smolikas trees and MXD data

The treeline ecotone on Mt. Smolikas contains a unique environmental archive hosting numerous 800 + year old Bosnian pines (*P. heldreichii*) as well as abundant relict trunks that have remained for centuries on the ground (Klippel et al. 2017). The *P. heldreichii* stands are situated between 2000 and 2200 m a.s.l. in relatively gentle terrain, though access to this ancient forest requires a longer hike through extended beech and black pine woods. Mt. Smolikas is the highest peak of the sparsely populated Pindus Range in northern Greece, where shallow soils on nutrient-poor serpentine bedrock, in concert with snowy winters and dry summers, provide ideal conditions for slow growing trees and limited wood decay.

Because of the site's high paleoclimatic potential, more than 700 core and disc samples from living and relict *P. heldreichii* were collected over the course of four field campaigns since 2013. From this collection, 192 cores and discs (taken from 103 trees) were selected to develop an evenly replicated MXD chronology extending back to early medieval times (Table 1). MXD is the maximum value of a high-resolution density profile in each ring, reflecting the ratio between the thickest cell walls and smallest cell lumens formed at the end of the growing season during late summer (Schweingruber et al. 1978). The data were produced at the tree-ring laboratory in Mainz (Germany) using a Walesch X-ray densitometer (Dendro-2003, Walesch Electronic). The Walesch technology supports the determination of absolute wood densities in g/cm^3, with sufficient resolution to work

Table 1 Mt. Smolikas MXD chronology characteristics. MXD age trend (bottom line) calculated over the first 500 years after aligning the data by cambial age (see Fig. 2a)

	Mt. Smolikas chronology
Latitude, longitude	40.1° N | 29.0° E
Elevation	2000–2200 m a.s.l.
Chronology period	574–2015 CE
Number of trees and radii	103 | 192
Mean series length	303 years
Mean pith offset	117 years
Interseries correlation	0.24
Average MXD	0.69 g/cm^3
Age trend per 100 years	−0.008 g/cm^3

with slow growing timberline trees that often produce only a few tracheid cell rows in single rings. The MXD values derived from Mt. Smolikas *P. heldreichii* radiodensitometric profiles range from 0.64–0.76 g/cm^3 with an average of 0.69 g/cm^3.

2.2 MXD chronology development, calibration and transfer

As characteristic for all conifer tree-ring density data (Briffa et al. 1998b; Büntgen et al. 2011; Davi et al. 2003; Esper et al. 2010, 2017; Frank and Esper 2005; Schweingruber and Briffa 1996), the individual *P. heldreichii* sample profiles contains a gentle, though persistent, age-trend of monotonically decreasing MXD values from ~0.72 to 0.68 g/cm^3 over the first 500 years of tree growth (Fig. 2). This age trend represents noise from a paleoclimatic perspective that requires removal via tree-ring detrending (Cook and Kairiukstis 1990). We here applied Regional Curve Standardization (RCS), a detrending technique designed for building composite chronologies that integrate samples from living trees and relict wood distributed over several centuries, and capable of preserving high-to-low frequency climate variability (Briffa et al. 1992; Esper et al. 2003). RCS utilizes the smoothed arithmetic mean of the age-aligned MXD data (the red curve in Fig. 2a) to remove age-trend from such a composite dataset. Note that this empirically derived regional curve represents the sample mean across centuries with consideration of any missing innermost rings, when they occur, in each core and disc sample. Inclusion of this so-called pith offset (PO) is responsible for the increasing trend in the replication curve over the first ~100 years of tree age (bottom panel of Fig. 2a). However, tests showed that consideration of PO (or not) has virtually no effect on the resulting RCS chronology, likely because of the rather small MXD age-trend of only −0.04 g/cm^3 over the first 500 years of tree growth.

The final RCS chronology was developed by calculating the arithmetic mean of the residuals between the MXD measurement series and the smoothed regional curve, after re-aligning the detrended series back to calendar years (Fig. 2b). The variance of this arithmetic mean was

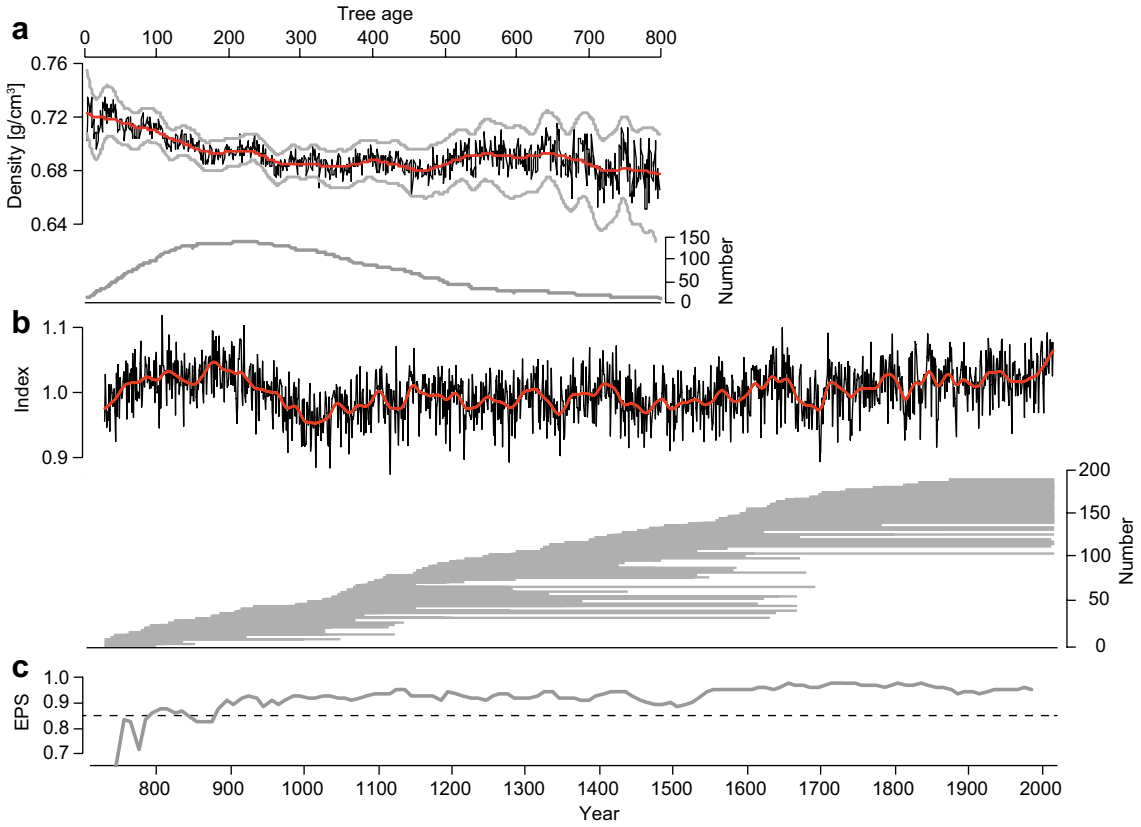

Fig. 2 MXD chronology development. **a** Arithmetic mean of the age-aligned MXD data (black curve) together with a 100-year spline low pass filter (red) and 30-year smoothed 95% bootstrap confidence intervals (grey). Bottom curve shows the sample replication over the first 800 years of cambial age. **b** The RCS-detrended MXD index chronology (black), its 30-year cubic smoothing spline (red), and distribution of measurement series sorted by their first ring since 730 CE (grey horizontal bars). **c** Expressed Population Signal (EPS) calculated over 50-year intervals shifted along the 730–2015 chronology period

stabilized using a 100-year running standard deviation approach applied to a high-pass filtered chronology version to account for temporal changes in sample replication and inter-series correlation (Frank et al. 2007). The chronology was truncated at a minimum replication of ten MXD series in 730 CE. The Expressed Population Signal (EPS, Wigley et al. 1984) was calculated over 50-year intervals shifted along the chronology to estimate temporal changes in signal strength related to declining sample replications and varying inter-series correlations (Fig. 2c).

The RCS chronology was calibrated against the nearest 100 + year temperature station in Larissa (Hansen et al. 2010), and against gridded temperature products integrating multiple station records of varying lengths (Rohde et al. 2013). Larissa is a near-coastal station located 230 km southeast and > 2000 m below the tree-ring sampling site in the Pindus Range, thereby providing conservative estimates of MXD signal strength, i.e. the temperature information encoded into the trees is likely underestimated owing to the significant horizontal and vertical distances. The record was split into two equally long periods (1911–1962 and 1963–2015) to estimate potential changes in signal strength considering the Pearson correlation coefficient, reduction of error (RE), and coefficient of efficiency (CE) statistics. Whereas RE determines if the proxy-based temperature estimates are better than the instrumental temperature mean in the calibration period, CE is an even more rigorous statistic referring to the instrumental mean of the verification period (Cook et al. 1994). RE and CE range from + 1 to $-\infty$, and positive values indicate reconstruction skill. The Durban–Watson statistic (DW) was additionally considered to assess autocorrelation in the residuals between the instrumental temperatures and regressed MXD chronology. DW values close to 2 indicate minor drift between the predictand and predictor (Durbin and Watson 1951). The final reconstruction was produced by scaling (Esper et al. 2005) the mean and variance of the RCS-detrended MXD chronology to the Larissa temperatures from 1911–2015, expressed as anomalies with respect to the 1961–1990 mean. Bootstrap confidence limits, derived from re-sampling and averaging the detrended MXD data with replacement 1000 times, were used for estimating a 95% confidence range of the reconstruction (Briffa et al. 1992). The bootstraps were smoothed using 30-year low pass filters to emphasize long-term confidence changes over the 730–2015 CE reconstruction period.

2.3 Benchmarking and climate model simulations

The new reconstruction from northern Greece was compared with high-resolution records from Fennoscandia (NEur) and the Alps (CEur) focusing on medieval temperature deviations (from 800–1200 CE) and on orbitally forced long-term trends. NEur is the world's current longest and best replicated MXD-based temperature reconstruction derived from high latitude (> 67° N) *Pinus sylvestris* trees in Finnish and Swedish Lapland (Esper et al. 2014). That record covers the entire Common Era, contains a strong June–August (JJA) temperature signal, and displays a millennial-scale cooling trend of − 0.31°/1000 years attributed to orbital forcing (Esper et al. 2012). CEur is the longest and best replicated MXD-based temperature reconstruction from central Europe derived from high-elevation (> 1600 m a.s.l.) *L. decidua* trees in the Swiss Alps (Büntgen et al. 2006). The record reaches back to 755 CE, displays a seasonally extended temperature signal from June–September (JJAS), and calibrates exceptionally well against regional temperature data reaching back to 1760 CE.

We analyzed these records from Fennoscandia, the Alps and Greece by plotting their correlation fields in ~ 50-year time slices since 1750 CE against gridded temperatures (Rohde et al. 2013), and by fitting least-squares linear regressions since 850 CE to evaluate millennial-scale temperature trends across Europe. These empirically derived long-term trends were additionally compared with the trends retained in a suite of orbitally forced and un-forced climate simulations from state-of-the-art climate models of the Paleoclimate Modelling Intercomparison Project (PMIP). Those include the CCSM4 (Gent et al. 2011), CESM (Lehner et al. 2015), GISS-E2R (Schmidt et al. 2014), and MPI-ESM (Zanchettin et al. 2013) models, from which seasonal temperature simulations were considered using the mean of two grid points in northern Europe (23.75° E and 25.00° E at 67.38° N), central Europe (7.50° E and 8.75° E at 46.65° N), and southern Europe (20.00° E and 21.25° E at 40.05° N), close to the reconstruction tree sites. Note that only the CESM run is devoid of any orbital forcing, whereas all other simulations are orbitally forced. In CESM, also the solar insolation amplitude is larger by a factor of two compared to CCSM4 (details in Lehner et al. 2015). The statistical significance of the least-squares regressions, fitted to the reconstructions and simulations, were estimated by applying a slope parameter test (von Storch and Zwiers 1999).

3 Results and discussion

3.1 MXD climate signal

The Mt. Smolikas MXD data contain a temperature signal covering the growing season from April to September including a distinct maximum from July–September (JAS) during which regional correlations exceed 0.5 (Fig. 3). The signal appears physiologically meaningful as secondary cell wall formation and lignification in the latewood of conifers growing in cold environments is reportedly controlled by high and late summer warmth in many sites across the

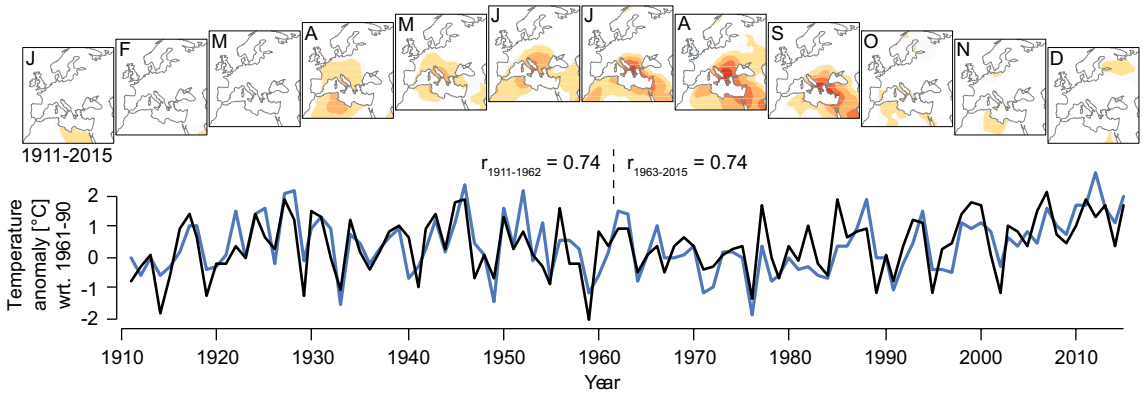

Fig. 3 MXD calibration. Monthly correlations of the MXD chronology against gridded temperature data (Berkeley; Rohde et al. 2013) from 1911–2015. Color scale as in Fig. 5. Bottom curves are the MXD chronology (black) shown together with the JAS temperature record from Larissa (blue)

Northern Hemisphere (Briffa et al. 1998b; Büntgen et al. 2011; Frank and Esper 2005; Schweingruber and Briffa 1996). Cell wall growth, and tangentially reduced lumen size, are the unique characteristics of conifer latewood tracheids (Carrer et al. 2018; Moser et al. 2010) controlling the inter-annual MXD variations of treeline *P. heldreichii* over the past 100 + years.

The Mt. Smolikas MXD chronology calibrates at r = 0.73 against JAS temperatures, from 1911–2015, recorded at Larissa (Fig. 3). This high level of coherency, representing ~ 53% of explained instrumental temperature variance, is surprising since the station's elevation is only 67 m a.s.l., located in one of the hottest cities in Greece that frequently experiences > 40 °C during summer, whereas the tree-ring data are from a remote mountain site at 2000–2200 m a.s.l. in northern Greece (Fig. 1). Additional tests considering 10-year high- and low-pass filtered proxy and instrumental data returned fairly balanced correlations ($r_{HP} = 0.70$, $r_{LP} = 0.81$) indicating signal strength at inter-annual to multi-decadal frequencies.

The Mt. Smolikas MXD correlation values are similar to those obtained for the MXD chronologies from *Pinus uncinata* in the Spanish Pyrenees ($r_{1950–2014} = 0.72$; Büntgen et al. 2017), *L. decidua* in the Swiss Alps ($r_{1818–2003} = 0.69$; Büntgen et al. 2006), and *P. sylvestris* in northern Scandinavia ($r_{1876–2006} = 0.77$; Esper et al. 2014), though the latter benefits from the comparison to more representative instrumental station data recorded in the relatively flat terrain of Fennoscandian Lapland. Other high-resolution temperature reconstructions from the Mediterranean, based on *L. decidua* TRW in the French Alps ($r_{1901–2002} = 0.53$) and *J. excelsa* $\delta^{13}C$ in the Turkish Taurus ($r_{1949–2006} = -0.52$), produce lower correlation coefficients (Büntgen et al. 2012; Heinrich et al. 2013).

Splitting the Larissa calibration period into two equal halves returns identical correlations ($r_{1911–1962}$ and $r_{1963–2015} = 0.74$), which suggests temporal robustness of the temperature signal retained in the Mt. Smolikas MXD data. This conclusion is supported by positive RE values ranging from 0.47–0.49, when regressing the MXD chronology against Larissa JAS temperatures over the early 1911–1962 and late 1963–2015 calibration/verification periods. The even more rigorous CE statistic (Cook et al. 1994) does not markedly undercut this range (0.47–0.48) as the calibration and verification period means are quite similar (0.41 °C and 0.33 °C w.r.t. 1961–1990). The Durban Watson statistic, testing for first-order autocorrelation in proxy-target residuals, relative to first-differenced timeseries, is 1.59, reinforcing the predictive skill of the modelled temperatures (Durbin and Watson 1951). These metrics, together with the basic correlation results, are in the range of the top-scoring millennial-length tree-ring reconstructions worldwide (Esper et al. 2016), and support the transfer of the RCS-detrended Mt. Smolikas MXD chronology into estimates of JAS temperatures back to 730 CE.

3.2 JAS temperature reconstruction

The Mt. Smolikas reconstruction shows warm temperatures towards the end of the first millennium CE, followed by a strong cooling trend in the tenth and early eleventh centuries, and a long-term, almost millennial-scale, warming trend culminating in the early twenty-first century (Fig. 4). These lower frequency changes are accompanied by marked decadal to multi-decadal scale fluctuations, such as the change from warmer to colder conditions during the seventeenth century, as well as numerous extremely cold and warm late summers recorded over the past 1286 years. Reconstruction skill is likely high throughout the second millennium CE as the number of MXD measurement series remains fairly stable and only changes from n = 56 in the twentieth century to n = 39 in the eleventh century (see the bottom panel in

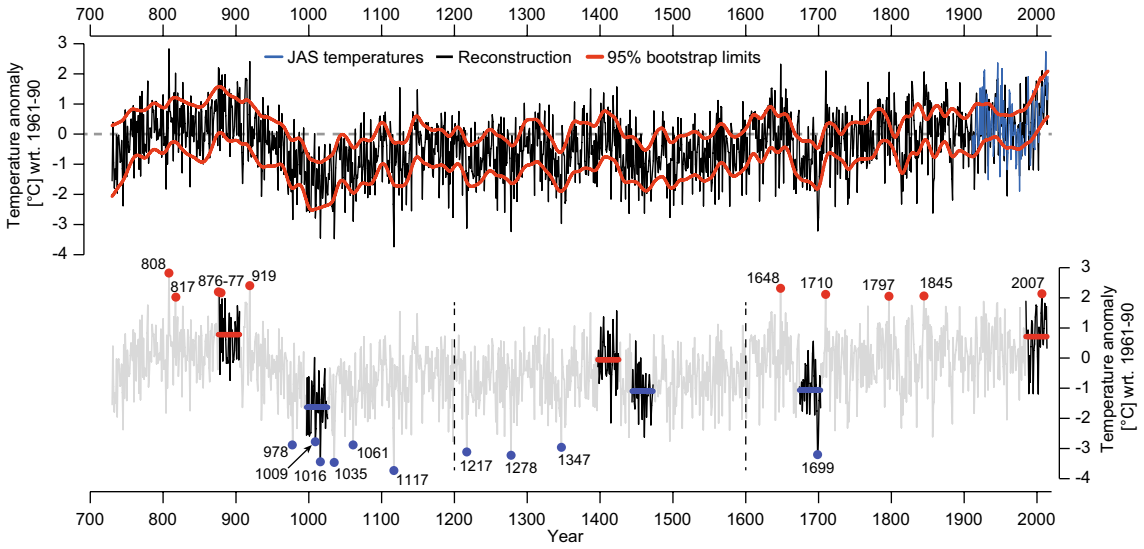

Fig. 4 Eastern Mediterranean temperature history and extremes. Mt. Smolikas MXD chronology (black curve) scaled against Larissa JAS temperatures (blue) together with 30-year smoothed 95% bootstrap confidence limits (red). Bottom panel shows the same reconstruction (grey) with the ten coldest and warmest years since 730 CE highlighted in red and blue, as well as the warmest and coldest 30-year periods before 1200 CE, from 1201–1600 CE, and after 1601 (red and blue horizontal lines)

Fig. 2b). Sample replication, however, then sharply declines and reaches a minimum of n = 10 series in 730 CE. This decline is illustrated by the running EPS statistic (Fig. 2c) dropping temporarily below 0.85 in the late ninth century, and deteriorating in the eighth century, revealing a reduction of reconstruction skill during these early chronology periods. The latter is characterized by an increased bootstrap confidence range in the ninth and eighth centuries (shown in red in Fig. 4a). However, the smoothed bootstrap confidence intervals also indicate that the warmer conditions during the late ninth century and the colder conditions during the early eleventh century differ significantly ($p < 0.05$) from the 1961–1990 mean (Table 2). The same is true for several subsequent cold periods over the past 900 years, as well as the recent warmth since the late twentieth century.

Considering the reconstruction mean timeseries, the warmest 30-year period since 730 CE occurred during high Medieval times (876–905 CE = + 0.78 °C w.r.t. 1961–1990) and has been slightly warmer than the recent period from 1985–2014 (+ 0.71 °C). The coldest 30-year period also falls in the Middle Ages (997–1026 = − 1.63 °C), colder than any other period during the Little Ice Age from 1400 to 1900 CE. The differences among cold periods and among warm periods are, however, all statistically insignificant as is highlighted by the bootstrap confidence range accompanying the reconstruction (Fig. 4b; Table 2). The reconstructed JAS extremes range from + 2.32 °C in 1648 CE (+ 2.82 °C in the less reliable year 808) to − 3.73 °C in 1117 CE revealing an overall temperature range exceeding 6.0 °C (6.5 °C), considering the reconstruction mean timeseries. These values are, however, sensitive to the statistical approach and the instrumental period used for transforming the MXD chronology into estimates of late summer temperature variability (see Esper et al. 2005 for details). For an assessment of single extreme years and significance of volcanic forcing see Klippel et al. (2019a), in which the authors applied different detrending methods to particularly emphasize high frequency variability in Mt. Smolikas MXD data.

Some constraints due to the calibration based on relatively short instrumental station data need to be considered when evaluating the millennial-length climate reconstruction. Whereas such a calibration provides an excellent perspective on the spatial patterns of temperature signals (e.g. Fig. 2a), reconstructed temperature deviations exceeding the variance of the instrumental period cannot fully be validated using classical calibration/verification techniques (von Storch et al. 2004). This is particularly the case for many of the cold periods reconstructed over the past 1000 + years that clearly go below the temperatures recorded during the warm twentieth and early twenty-first centuries. The same is true for the reconstructed millennial-scale trend, which seemingly extends beyond anything recorded during the relatively short instrumental period (see Sect. 3.3).

Given that the TRW data from the same Smolikas trees are sensitive to hydroclimate variability, not temperature (Klippel et al. 2018), the nearest possible proxy validation afforded is with a recently published JAS temperature reconstruction from Mt. Olympus about 120 km west of Mt. Smolikas (Klesse et al. 2015). That reconstruction, also derived from high elevation *P. heldreichii* MXD, but extending

Table 2 Reconstructed temperature extremes

	30-Year period	JAS temperature (°C)	95% interval (°C)
Pre-1200	876–905	+0.78	±0.74
	997–1026	−1.63	±0.79
1201–1600	1397–1426	−0.06	±0.74
	1444–1473	−1.10	±0.70
Post-1600	1985–2014	+0.71	±0.51
	1647–1703	−1.06	±0.69
	Years		
Ten warmest late summers	808	+2.82	±0.68
	919	+2.40	±0.72
	1648	+2.32	±0.59
	876	+2.20	±0.85
	877	+2.15	±0.81
	2007	+2.10	±0.48
	1710	+2.09	±0.67
	1845	+2.06	±0.55
	1797	+2.05	±0.59
	817	+2.02	±0.64
Ten coldest late summers	1117	−3.73	±0.64
	1035	−3.47	±0.78
	1016	−3.44	±0.60
	1278	−3.23	±0.64
	1699	−3.21	±0.77
	1217	−3.12	±0.58
	1347	−2.96	±0.79
	1061	−2.89	±0.74
	978	−2.83	±0.78
	1009	−2.78	±0.72

Warmest and coldest 30-year periods pre-1200, 1201–1600 and post 1600, and ten warmest and coldest reconstructed late summers since 730 CE, together with their 95% bootstrap confidence intervals. All temperatures expressed in °C with respect to the 1961–1990 climatology

back to only 1521 CE, correlates exceptionally well with our record over the recent 245-year period of overlap since 1766 ($r_{1766–2010} = 0.82$). The correlation then declines over the early 245-year period of overlap, but is still highly significant ($r_{1510–1765} = 0.67$, $p < 0.01$). This drop in correlation is likely due to the reduced sample size in the early period of the Mt. Olympus MXD chronology (Klesse et al. 2015). Coherency between the two reconstructions reinforces the skill of our new record at inter-annual to multi-decadal scales. However, the Mt. Olympus chronology is too short to validate the millennial-scale warming trend retained in the Mt. Smolikas chronology.

3.3 Millennial-scale temperature trends

The millennial-scale warming trend recorded in northern Greece is a new feature of Mediterranean climate variability. By a least-squares linear regression fit over the full 730–2015 CE reconstruction period the trend equals +0.31 °C/1000 years. The trend is robust with respect to the MXD detrending method, i.e. chronology variants produced using different RCS specifications (Esper et al. 2003) and signal free detrending (Melvin and Briffa 2008) are all highly similar, likely due to the trifling age trend inherent in the *P. heldreichii* MXD data (−0.008 g/cm^3 per 100 years). Because this observed long-term warming cannot be validated against any equally long regional high-resolution temperature reconstructions, we compare our record from northern Greece (SEur hereafter) with MXD-based temperature reconstructions from Scandinavia (NEur) and the Alps (CEur; Fig. 5), as well as temperature simulations from state-of-the-art climate models (Fig. 6). Reconstructions derived from TRW are not considered, because this parameter is limited in its ability to retain millennial-scale temperature trends (Esper et al. 2012; Klippel et al. 2019b).

The three MXD-based reconstructions (NEur, CEur, SEur) all calibrate exceptionally well against observational data, though comparison with gridded temperatures back to

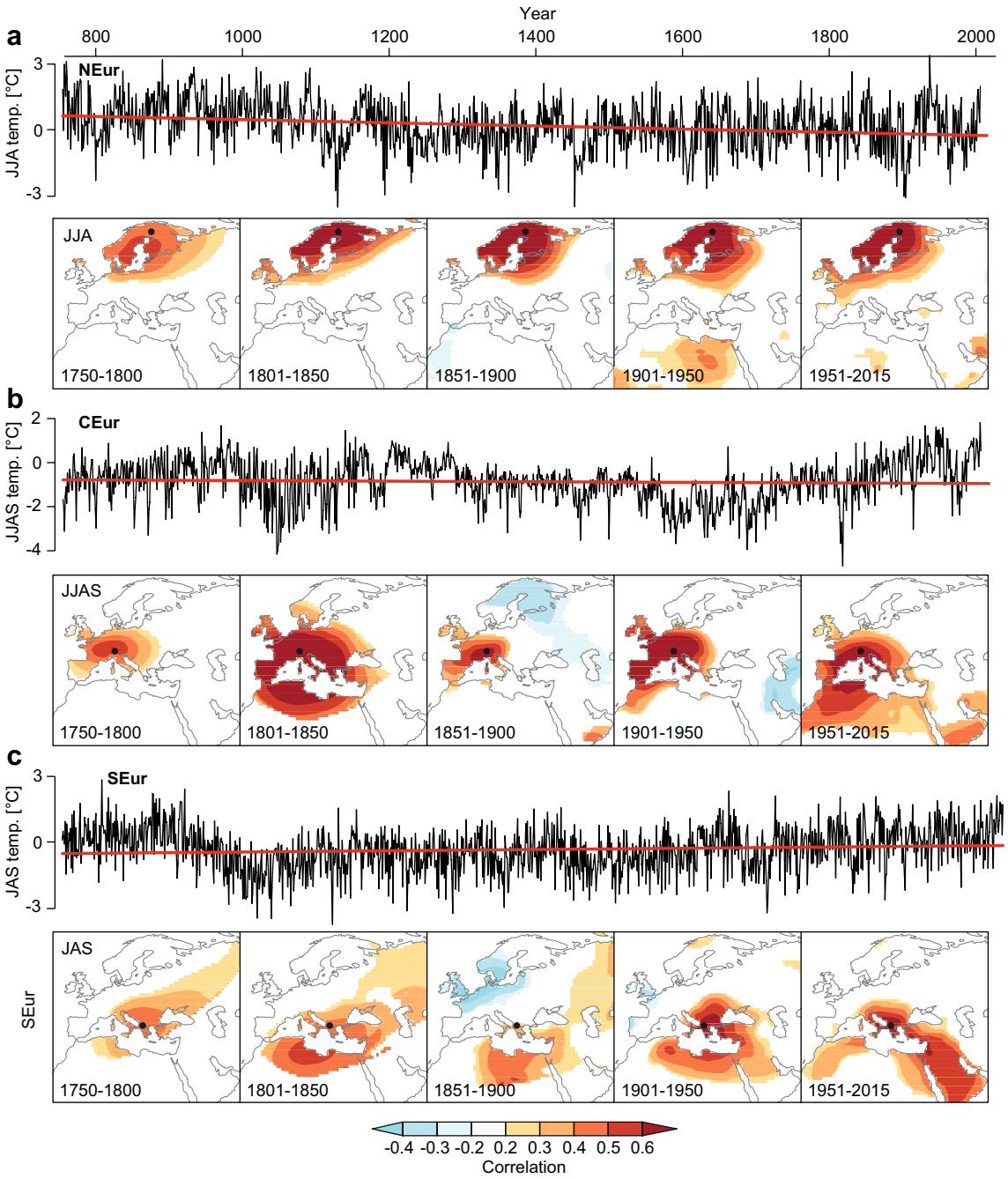

Fig. 5 Millennial-scale MXD-based temperature reconstructions across Europe. **a** The NEur JJA temperature reconstruction from northern Fennoscandia (black curve, from Esper et al. 2014) together with a least-squares linear regression fit from 755–2006 CE (red). Bottom panel shows correlation fields against instrumental JJA temperatures (Rohde et al. 2013) during five distinct periods since 1750 CE. **b** The CEur JJAS temperature reconstruction from the Swiss Alps (Büntgen et al. 2006), regression from 755–2004, and JJAS correlations fields. **c** The SEur reconstruction (this study), regression from 755–2015, and JAS correlation fields

1750 CE indicates a general weakening of correlation fields back in time (the bottom panels in Fig. 5a–c). This decline is likely not related to deficiencies in the reconstructions, which all rely on well-replicated MXD chronologies over the past 250 years, but rather a weakening of the instrumental station network back in time (except for the 1801–1850 field in CEur; Fig. 5b). The gridded instrumental data used here (Rohde et al. 2013) include 31 temperature stations from Greece, the longest of these records extends back to only 1858 (Athens), and there is no station record within a 1000 km search radius from the tree-ring site extending back to 1750. In addition, of the 2127 European stations used to

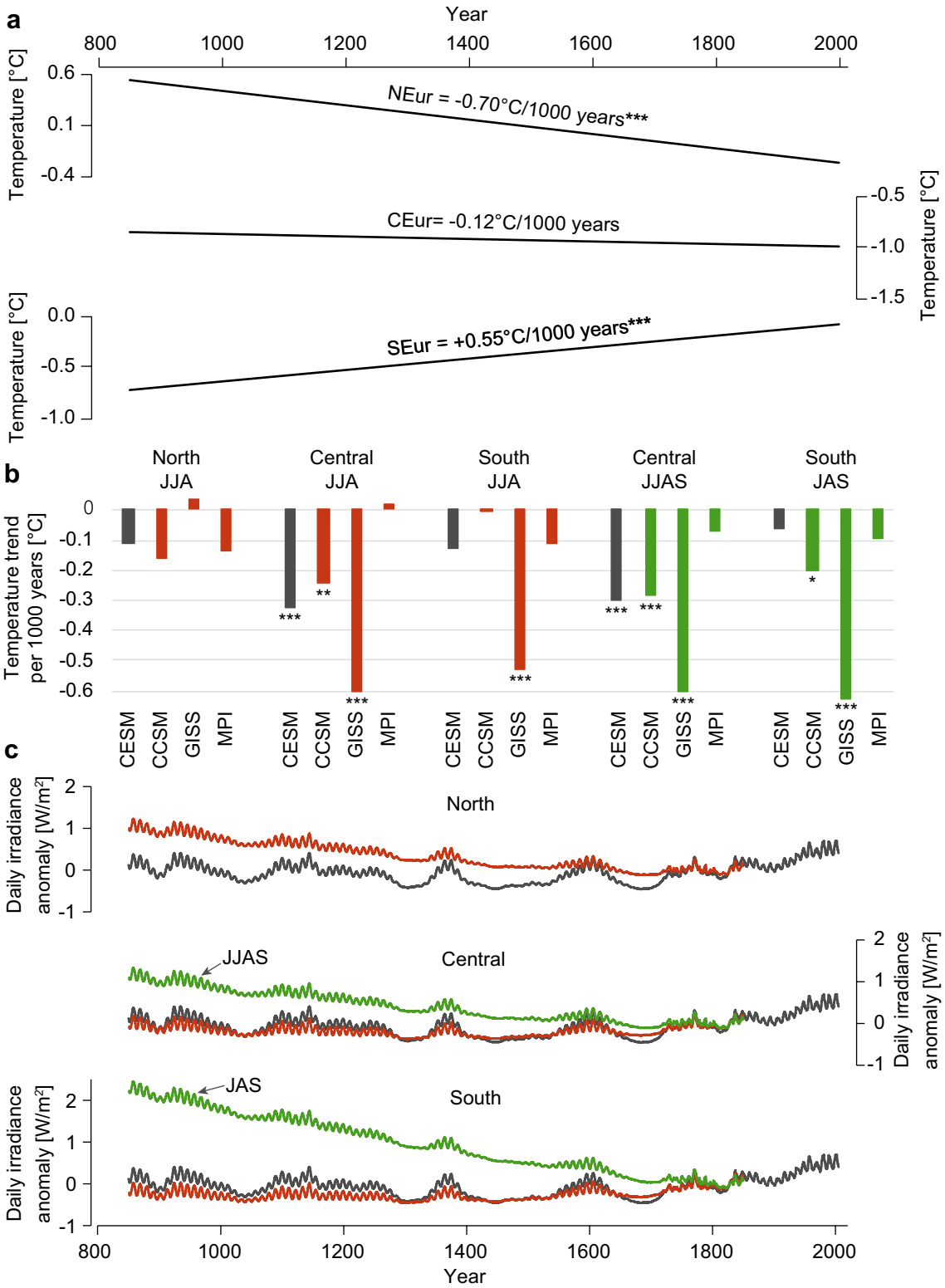

produce the interpolated field, only three stations (De Bilt, Uppsala, Berlin) reach back to 1750, and only three stations south of the Alps include observations prior to 1800: Torino (back to 1753 with gaps), Milano (1763), and Padova (1774).

While the correlation fields, and their temporal decay, nicely illustrate the strength of the climate signal in the proxy records and instrumental network, they can hardly validate the differing millennial-scale temperature trends

◂**Fig. 6** Reconstructed and simulated temperatures trends. **a** Least-squares linear regressions fit to the NEur, CEur, and SEur temperature reconstructions from 850–2005 CE. Statistically significant ($p < 0.001$) regression slopes are marked with *** (von Storch and Zwiers 1999). **b** The regression slopes from fits against the CESM, CCSM4, GISS, and MPI temperature simulations from 850–2005 CE in northern, central and southern Europe considering different seasons (JJA, JJAS, JAS). The colors refer to basic differences in forcing, including black for no orbital forcing (CESM), red for orbital forcing during JJA, and green for orbital forcing during JJAS (central) and JAS (south). Regression slopes significant at $p < 0.001$ marked with ***, $p < 0.01$ with **, $p < 0.05$ with *. **c** Solar insolation anomalies (W/m^2 relative to the 1800–1850 mean) with time-varying orbital parameters as used in CCSM4 (red and green) and with fixed orbital parameters as used in CESM (black). Black and red refer to JJA, green shows additional trends for JJAS in central and JAS in southern Europe. The increased decadal scale variability in the CESM forcing (black) results from upscaling insolation variance including the synthetic 11-year solar cycle to account for recently increased estimates (details in Lehner et al. 2015)

across Europe. When calculated over 850–2004 CE, the common period of overlap amongst the reconstructions and climate model simulations, these trends range from −0.70 °C/1000 years in NEur, to −0.12 °C/1000 years in CEur, and +0.55 °C/1000 years in SEur (Fig. 6a). A regression slope parameter test reveals the negative trend in NEur and the positive trend in SEur to be statistically significant at $p < 0.001$ (von Storch and Zwiers 1999). However, the linear trend values presented here are sensitive to end effects and changes in timeseries length, e.g. the SEur trend changes from +0.31 °C (730–2015) to +0.55 °C/1000 years (850–2004) when curtailing the relatively warm eighth and early ninth centuries.

The changing long-term trends from NEur to CEur to SEur appear meaningful, if we consider the weakening of high summer (typically July 15) orbital forcing from high to mid latitudes (Wanner et al. 2008). However, a more detailed assessment including several state-of-the-art climate models and seasonal orbital forcing reveals no coherency between the simulated and empirical trends, nor among the model runs (Fig. 6b, c): (1) the trends in one model change from slightly positive (+0.03 °C/1000 years) to significantly negative (−0.61 °C/1000 years, $p < 0.001$) while the negative orbital forcing diminishes (GISS during JJA in northern and central Europe); (2) the trends in another model remain close to zero (from +0.02 to −0.14 °C/1000 years) while substantial latitudinal and seasonal changes in orbital forcing occurred (MPI during JJA, JJAS and JAS); and (3) even though a run is conducted using fixed orbital parameters (CESM, black curves in Fig. 6c) a model can produce persistently negative trends (from −0.07 to −0.33 °C/1000 years, $p < 0.001$). Some simulations might also be affected by artificial drifts from not fully equilibrated starting conditions. The models therefore paint an inconsistent picture of low frequency temperature histories, fully liberated from orbital forcing, which cannot be used to validate (or falsify) the spatially changing temperature trends in the empirical reconstructions. In addition, the proxy-based trends do not cohere with the spatially and seasonally changing orbital forcing trends. This latter conclusion has to be considered with caution though, as the designated seasons of temperature signals (JJA in NEur, JJAS in CEur, JAS in SEur) were established via calibration against relatively short instrumental data, an approach that typically ignores additional sensitivities to earlier and later months (e.g. the correlation fields in April, May and June in Fig. 2a).

3.4 Medieval temperature variability

Another striking feature of the Mt. Smolikas reconstruction is the severe tenth century cooling trend culminating in a record low of −1.63 °C from 997–1026 CE (Figs. 4, 7; Table 2). This period falls right into the center of the MWP, which has been shown in several large-scale reconstructions to be substantially warmer than the subsequent Little Ice Age (Anchukaitis et al. 2017; Schneider et al. 2015; Stoffel et al. 2015; Wilson et al. 2016), albeit the number of tree-ring series included in these hemispheric products declines dramatically back in time (Esper et al. 2018). The distinct MWP cold phase in northern Greece is thus an uncommon feature in the Northern Hemisphere extratropics, though lower-resolution historical-climatological information from around Constantinople supports the notion of regionally cold (and dry) summers in the early eleventh century in the northeastern Mediterranean (Xoplaki et al. 2016). This conclusion is based on a systematic collection of Byzantine textual evidence including reports on harvest failure, plague outbreaks, and demographic responses (Telelis 2008).

Additional assessments against regional high-resolution summer temperature reconstructions, extrapolated from a European network of calibrated and verified proxies at 5° resolution (Luterbacher et al. 2016), are restricted by the lack of predictors from the eastern Mediterranean region. In fact, the northern Greece grid point reconstruction, representing 37.5–42.5 N and 17.5–22.5 E of the Luterbacher et al. (2016) network, correlates only at $r_{800–2003} = 0.13$ with the SEur temperature reconstruction from Mt. Smolikas, but at $r_{800–2003} = 0.73$ with the CEur reconstruction from the Swiss Alps. CEur is one the predictor reconstructions used in Luterbacher et al. (2016). The importance of CEur as a predictor of temperature variability in the eastern Mediterranean even increases back in time, as is documented by the very high correlation with the northern Greece grid point reconstruction prior to 1200 CE ($r_{800–1200} = 0.89$). These values demonstrate that the climate field reconstructions in the eastern Mediterranean are currently dominated by non-Mediterranean predictors (Luterbacher et al. 2016). It is thus advisable to directly compare SEur with CEur (and NEur)

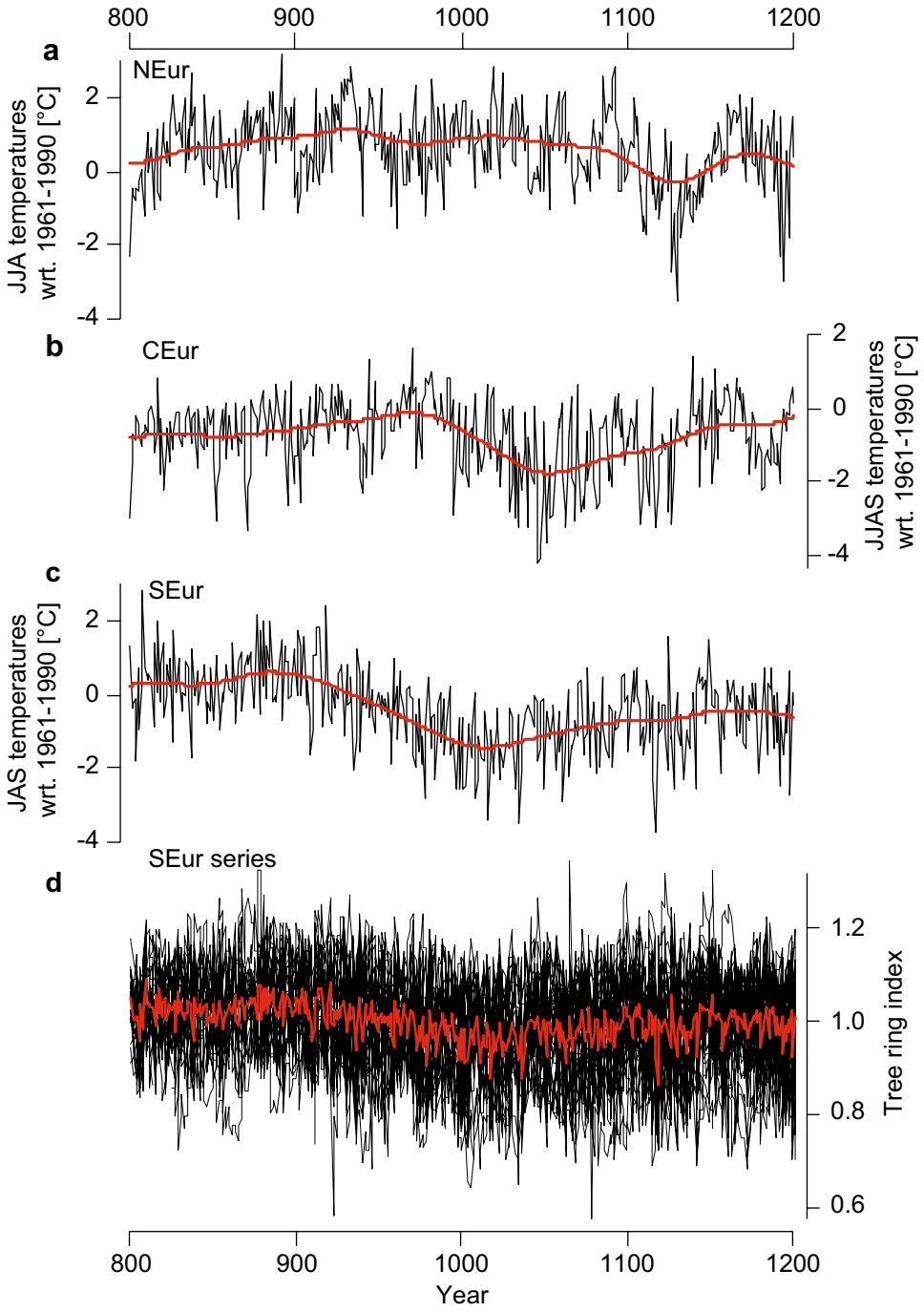

Fig. 7 Medieval temperature estimates 800-1200 CE from European MXD records. **a**–**c** Warm season temperature reconstructions from Northern Scandinavia (NEur), the Alps (CEur), and Greece (SEur). Red curves are 100-year splines. **d** RCS-detrended MXD measurement series from SEur and their arithmetic mean (red)

to evaluate medieval temperature variability across Europe and avoid circular reasoning.

Considering the MXD-based temperature reconstructions from northern and central Europe reveals that a distinct cold period, such as recorded from 997–1026 CE in SEur, was not unique in medieval Europe (Fig. 7). Whereas the smoothed NEur reconstruction (red curve in Fig. 7a) remains above the 1961–1990 mean throughout most of the ninth to twelfth centuries, a distinct cold swing is recorded in the mid eleventh century in CEur (− 2.04 °C from 1029–1058 CE). However, this period is additionally characterized by an increase in inter-annual variability, likely driven by a higher inter-series correlation among MXD series from a single historical building in the Simplon valley, Switzerland (see Büntgen et al. 2006 for details). The fact that the medieval portion of the CEur chronology originates from the Simplon valley, whereas all post-1200 CE data are from the neighboring Lötschental, is a weak point in this otherwise high quality millennial-length temperature reconstruction (Esper et al. 2016). The new record from Mt. Smolikas now provides

more perspective on the MWP and reinforces the notion that severe cold episodes occurred in medieval Europe. However, the cold MWP episodes in SEur and CEur are not exactly in phase, and were dynamically likely of different origin considering current weather patterns and air mass dynamics (Xoplaki et al. 2003).

Further comparison with reconstructions of total solar irradiance (TSI, Vieira and Solanki 2010) and volcanic activity (Gao et al. 2008; Toohey and Sigl 2017) indicates that these external climate forcings are of limited use to explain the MPW temperature patterns across Europe (Fig. 8), suggesting that random, internal variability was dominating

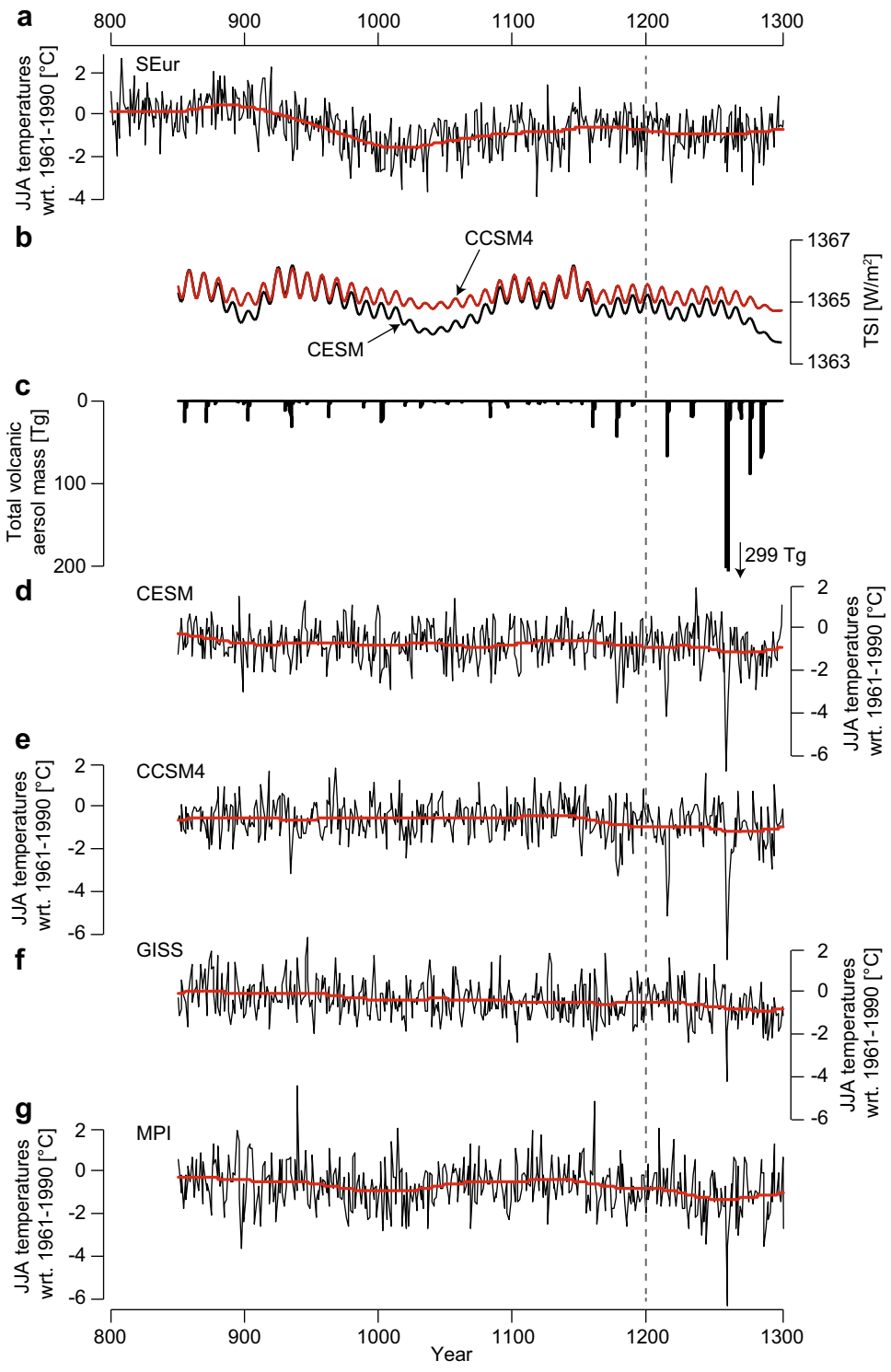

Fig. 8 Warm season temperatures and forcing from 800–1300 CE. **a** JAS temperature reconstruction from northern Greece (SEur). Red curve is a 100-year spline. Vertical dashed line marks the period until 1200 CE shown in Fig. 7. **b**, **c** Total solar irradiance and volcanic aerosol mass forcing timeseries as used in the CCSM4 and CESM models. **d**–**g** Four SEur JAS temperature simulations from the CESM, CCSM4, GISS and MPI models (black) and 100-splines (red)

(Xoplaki et al. 2018). The TSI reconstruction shows lower values in the mid eleventh century, particularly in the CESM forcing timeseries that was increased by a factor of two (Lehner et al. 2015), but these changes are overall still small and remain within an envelope of only 2 W/m^2. Similarly, the Middle Ages, and particularly the eleventh century, were a quiet period with respect to volcanic forcing, as the large eruptions, exceeding aerosol masses of 60 Tg, did not kick in again until the mid thirteenth century (Gao et al. 2008). The overall weak solar and volcanic forcings during MWP are also reflected in the climate model runs showing no substantial temperature variability at multi-decadal timescales before 1200 CE (Fig. 8d–g). On the other hand, the much stronger post-1200 CE volcanic forcing, including the 1257 Samalas eruption that released 300 Tg of volcanic aerosols, initiated much stronger, inter-annual to decadal scale temperature variability in the model simulations. Both of these features, the relatively quiet MWP conditions and the subsequently highly variable thirteenth century temperatures in the simulations, are thus not supported by the new JAS temperature reconstruction from Mt. Smolikas (see Klippel et al. 2019a; for an assessment of post-volcanic cooling events in northern Greece). However, for a more conclusive picture of Mediterranean climate variability and forcing during medieval times, additional high-resolution temperature reconstructions as well as improved climate forcing reconstructions (Steinhilber et al. 2012; Vieira and Solanki 2010) are needed.

4 Conclusions

Using high-resolution MXD data from an ancient *P. heldreichii* stand in northern Greece, we developed a late summer temperature reconstruction extending back to 730 CE. The reconstruction contains two features that are new to Mediterranean climate: (1) a millennial-scale warming trend in the order of + 0.3 °C/1000 years, and (2) a decadal-scale, exceptionally cold period during high medieval times (997–1026 = − 1.63 °C w.r.t. 1961–1990). Both these features are difficult to assess as properly calibrated, high-resolution temperature reconstructions extending back into the Medieval Warm Period are lacking from the Mediterranean region. Comparisons with similar high-resolution, robustly verified MXD reconstructions from Scandinavia and the Alps showed that millennial-scale temperature trends change from negative to positive from northern to central to southern Europe. However, these trends cannot be validated using climate simulations, as the model-derived temperature estimates neither cohere with orbital forcing nor among the different models. Similarly, the distinct cold spell recorded during high Medieval times in northern Greece appears to be unrelated to external climate forcings. A comparable temperature deviation is, however, seen slightly later in the Swiss Alps, demonstrating that such cold spells can occur during MWP and might be a genuine feature of eastern Mediterranean climate variability deserving attention in further studies.

Acknowledgements We thank Robert Brandes for pointing towards old-growth forest sites in Greece, and Markus Kochbeck, Yannik Esser, Eileen Kuhl and Philipp Römer for MXD measurements. Supported by the German Science Foundation projects "Inst 247/665-1 FUGG" and "ES 161/9-1".

References

Anchukaitis KJ et al (2017) Last millennium Northern hemisphere summer temperatures from tree rings: part II, spatially resolved reconstructions. Quat Sci Rev 163:1–22

Briffa KR, Jones PD, Bartholin TS, Eckstein D, Schweingruber FH, Karlen W, Zetterberg P, Eronen M (1992) Fennoscandian summers from AD 500: temperature changes on short and long timescales. Clim Dyn 7:111–119

Briffa KR, Jones PD, Schweingruber FH, Osborn TJ (1998a) Influence of volcanic eruptions on Northern Hemisphere summer temperature over the past 600 years. Nature 393:450–455

Briffa KR, Schweingruber FH, Jones PD, Osborn TJ, Shiyatov SG, Vaganov EA (1998b) Reduced sensitivity of recent tree-growth to temperature at high northern latitudes. Nature 391:678–682

Briffa KR, Melvin TM, Osborn TJ, Hantemirov RM, Kirdyanov AV, Mazepa VS, Shiyatov SG, Esper J (2013) Reassessing the evidence for tree- growth and inferred temperature change during the Common Era in Yamalia, Northwest Siberia. Quat Sci Rev 72:83–107

Büntgen U, Frank DC, Nievergelt D, Esper J (2006) Summer temperature variations in the European Alps, A.D. 755–2004. J Clim 19:5606–5623

Büntgen U, Frank DC, Grudd H, Esper J (2008) Long-term summer temperature variations in the Pyrenees. Clim Dyn 31:615–631

Büntgen U, Raible CC, Frank D, Samuli H, Cunningham L, Hofer D, Nievergelt D, Verstege A, Timonen M, Stenseth NC, Esper J (2011) Causes and consequences of past and projected Scandinavian summer temperatures, 500–2100 AD. PLoS One 6:e25133

Büntgen U, Neuschwander T, Frank D, Esper J (2012) Fading temperature sensitivity of Alpine tree growth at its Mediterranean margin and associated effects on large-scale climate reconstructions. Clim Change 114:651–666

Büntgen U et al (2017) New tree-ring evidence from the Pyrenees reveals Western Mediterranean climate variability since medieval times. J Clim 30:5295–5318

Büntgen U et al (2018) Tree rings reveal globally coherent signature of cosmogenic radiocarbon events in 774 and 993 CE. Nat Commun 9:3605

Carrer M, Unterholzner L, Castagneri D (2018) Wood anatomical traits highlight complex temperature influence on *Pinus cembra* at high elevation in the Eastern Alps. Int J Biometeorol 62:1745–1753

Cook ER, Kairiukstis LA (1990) Methods of dendrochronology. Applications in the Environmental Science. Kluwer, Dordrecht

Cook ER, Briffa KR, Jones PD (1994) Spatial regression methods in dendroclimatology: a review and comparison of two techniques. Int J Climatol 14:379–402

Davi NK, Jacoby GC, Wiles GC (2003) Boreal temperature variability inferred from maximum latewood density and tree-ring width data, Wrangell Mountain region, Alaska. Quat Res 60:252–262

Durbin J, Watson GS (1951) Testing for serial correlation in least squares regression. II. Biometrika 38:159–178
Esper J, Frank DC (2009) The IPCC on a heterogeneous Medieval Warm Period. Clim Change 94:267–273
Esper J, Cook ER, Krusic PJ, Peters K, Schweingruber FH (2003) Tests of the RCS method for preserving low-frequency variability in long tree-ring chronologies. Tree-Ring Res 59:81–98
Esper J, Frank DC, Wilson RJS, Briffa KR (2005) Effect of scaling and regression on reconstructed temperature amplitude for the past millennium. Geophys Res Lett 32:7
Esper J, Frank DC, Büntgen U, Verstege A, Luterbacher J, Xoplaki E (2007) Long-term drought severity variations in Morocco. Geophys Res Lett 34:17
Esper J, Frank DC, Büntgen U, Verstege A, Hantemirov RM, Kirdyanov AV (2010) Trends and uncertainties in Siberian indicators of 20th century warming. Glob Change Biol 16:386–398
Esper J, Frank DC, Timonen M, Zorita E, Wilson RJS, Luterbacher J, Holzkämper S, Fischer N, Wagner S, Nievergelt D, Verstege A, Büntgen U (2012) Orbital forcing of tree-ring data. Nat Clim Change 2:862–866
Esper J, Düthorn E, Krusic P, Timonen M, Büntgen U (2014) Northern European summer temperature variations over the Common Era from integrated tree-ring density records. J Quat Sci 29:487–494
Esper J, Schneider L, Smerdon J, Schöne B, Büntgen U (2015a) Signals and memory in tree-ring width and density data. Dendrochronologia 35:62–70
Esper J, Konter O, Krusic P, Saurer M, Holzkämper S, Büntgen U (2015b) Long-term summer temperature variations in the Pyrenees from detrended stable carbon isotopes. Geochronometria 42:53–59
Esper J et al (2016) Ranking of tree-ring based temperature reconstructions of the past millennium. Quat Sci Rev 145:134–151
Esper J, Büntgen U, Hartl-Meier C, Oppenheimer C, Schneider L (2017) Northern Hemisphere temperature anomalies during the 1450 s period of ambiguous volcanic forcing. Bull Volcanol 79:41
Esper J, St. George S, Anchukaitis K, D'Arrigo R, Ljungqvist F, Luterbacher J, Schneider L, Stoffel M, Wilson R, Büntgen U (2018) Large-scale, millennial-length temperature reconstructions from tree-rings. Dendrochronologia 50:81–90
Frank D, Esper J (2005) Characterization and climate response patterns of a high-elevation, multi-species tree-ring network in the European Alps. Dendrochronologia 22:107–121
Frank D, Esper J, Cook ER (2007) Adjustment for proxy number and coherence in a large-scale temperature reconstruction. Geophys Res Lett 34:16
Franke J, Frank DC, Raible CC, Esper J (2013) Spectral biases in tree-ring climate proxies. Nat Clim Change 3:360–364
Gao CC, Robock A, Ammann C (2008) Volcanic forcing of climate over the past 1500 years: an improved ice core-based index for climate models. J Geophys Res 113:D23
Gent PR et al (2011) The community climate system model version 4. J Clim 24:4973–4991
Griggs CB, Degaetano AT, Kuniholm PI, Newton MW (2007) A regional reconstruction of May-June precipitation in the north Aegean from oak tree-rings, AD 1089–1989. Int J Climatol 27:1075–1089
Grudd H (2008) Torneträsk tree-ring width and density AD 500–2004: a test of climatic sensitivity and a new 1500-year reconstruction of north Fennoscandian summers. Clim Dyn 31:843–857
Hansen J, Ruedy R, Sato M, Lo K (2010) Global surface temperature change. Rev Geophys 48:4
Heinrich I, Touchan R, Liñán ID, Vos H, Helle G (2013) Winter-to-spring temperature dynamics in Turkey derived from tree rings since AD 1125. Clim Dyn 41:1685–1701
Jones P et al (2009) High-resolution paleoclimatology of the last millennium: a review of current status and future prospects. Holocene 19:3–49
Klesse S, Ziehmer M, Rousakis G, Trouet V, Frank D (2015) Synoptic drivers of 400 years of summer temperature and precipitation variability on Mt. Olympus, Greece. Clim Dyn 45:807–824
Klippel L, Krusic PJ, Brandes R, Hartl-Meier C, Trouet V, Meko M, Esper J (2017) High-elevation inter-site differences in Mount Smolikas tree-ring width data. Dendrochronologia 44:164–173
Klippel L, Krusic PJ, Brandes R, Hartl C, Belmecheri S, Dienst M, Esper J (2018) A 1286-year hydro-climate reconstruction for the Balkan Peninsula. Boreas 47:1218–1229
Klippel L, Krusic PJ, Konter O, St. George S, Trouet V, Esper J (2019a) A 1200+ year reconstruction of temperature extremes for the northeastern Mediterranean region. Int J Climatol 39:2336–2350
Klippel L, St George S, Büntgen U, Krusic P, Esper J (2019b) Differing pre-industrial cooling trends between tree-rings and lower-resolution temperature proxies. Clim Past Discuss. https://doi.org/10.5194/cp-2019-41
Konter O, Krusic PJ, Trouet V, Esper J (2017) Meet Adonis, Europe's oldest dendrochronologically dated tree. Dendrochronologia 42:12
Lamb HH (1965) The early medieval warm epoch and its sequel. Palaeogeogr Palaeoclimatol Palaeoecol 1:13–37
Lehner F, Joos F, Raible CC, Mignot J, Born A, Keller KM, Stocker TF (2015) Climate and carbon cycle dynamics in a CESM simulation from 850 to 2100 CE. Earth Syst Dyn 6:411–434
Luckman BH, Wilson RJS (2005) Summer temperatures in the Canadian Rockies during the last millennium: a revised record. Clim Dyn 24:131–144
Luterbacher J et al (2012) A review of 2000 years of paleoclimatic evidence in the Mediterranean. In: Lionello P (ed) The climate of the Mediterranean region: from the Past to the Future. Elsevier, Amsterdam, pp 87–185
Luterbacher J et al (2016) European summer temperatures since Roman times. Environ Res Lett 11:024001
McKee TB, Doesken NJ, Kleist J (1993) The relationship of drought frequency and duration to time scales. In: Eighth conference on applied climatology. Colorado State University, Anaheim, pp 179–184
Melvin TM, Briffa KR (2008) A "signal-free" approach to dendroclimatic standardisation. Dendrochronologia 26:71–86
Melvin TM, Grudd H, Briffa KR (2013) Potential bias in 'updating' tree-ring chronologies using Regional Curve Standardization: re-processing the Torneträsk maximum-latewood-density data. Holocene 23:364–373
Moser L, Fonti P, Büntgen U, Esper J, Luterbacher J, Franzen J, Frank D (2010) Timing and duration of European larch growing season along an altitudinal gradient in the Swiss Alps. Tree Phys 30:225–233
Rohde R, Muller R, Jacobsen R, Perlmutter S, Rosenfeld A, Wurtele J, Curry J, Wickham C, Mosher S (2013) Berkeley earth temperature averaging process. Geoinform Geostat Overv 1:1–13
Schmidt GA et al (2014) Configuration and assessment of the GISS ModelE2 contributions to the CMIP5 archive. J Adv Model Earth Syst 6:141–184
Schneider L, Smerdon JE, Büntgen U, Wilson RJ, Myglan VS, Kirdyanov AV, Esper J (2015) Revising midlatitude summer temperatures back to AD 600 based on a wood density network. Geophys Res Lett 42:4556–4562
Schweingruber FH, Briffa KR (1996) Tree-ring density networks for climate reconstruction. In: Jones PD et al (eds) Climatic variations and forcing mechanisms of the last 2000 years. Springer, Berlin, pp 43–66
Schweingruber FH, Fritts HC, Bräker OU, Drew LG, Schär E (1978) The X-ray technique as applied to dendroclimatology. Tree Ring Bull 38:61–91

Schweingruber FH, Bartholin T, Schär E, Briffa K (1988) Radiodensitometric-dendroclimatological conifer chronologies from Lapland (Scandinavia) and the Alps (Switzerland). Boreas 17:559–566

Steinhilber F et al (2012) 9,400 years of cosmic radiation and solar activity from ice cores and tree rings. Proc Natl Acad Sci 109:5967–5971

Stoffel M et al (2015) Estimates of volcanic-induced cooling in the Northern Hemisphere over the past 1,500 years. Nat Geosci 8:784–788

Szymczak S, Hetzer T, Bräuning A, Joachimski MM, Leuschner HH, Kuhlemann J (2014) Combining wood anatomy and stable isotope variations in a 600-year multi-parameter climate reconstruction from Corsican black pine. Quat Sci Rev 101:146–158

Telelis IG (2008) Climatic fluctuations in the Eastern Mediterranean and the Middle East AD 300–1500 from Byzantine documentary and proxy physical paleoclimatic evidence. Jahrb Oesterreichischen Byz 58:167–207

Toohey M, Sigl M (2017) Volcanic stratospheric sulfur injections and aerosol optical depth from 500 BCE to 1900 CE. Earth Syst Sci Data 9:809–831

Touchan R, Akkemik Ü, Hughes MK, Erkan N (2007) May–June precipitation reconstruction of southwestern Anatolia, Turkey during the last 900 years from tree rings. Quat Res 68:196–202

Touchan R, Anchukaitis KJ, Meko DM, Attalah S, Baisan C, Aloui A (2008) Long term context for recent drought in northwestern Africa. Geophys Res Lett 35:13

Touchan R, Anchukaitis KJ, Meko DM, Sabir M, Attalah S, Aloui A (2011) Spatiotemporal drought variability in northwestern Africa over the last nine centuries. Clim Dyn 37:237–252

Vieira LEA, Solanki SK (2010) Evolution of the solar magnetic flux on time scales of years to millennia. Astronom Astrophys 509:A100

von Storch H, Zwiers FW (1999) Statistical analyses in climate research. Cambridge University Press, Cambridge

von Storch H, Zorita E, Jones JM, Dimitriev Y, González-Rouco F, Tett SF (2004) Reconstructing past climate from noisy data. Science 306:679–682

Wanner H et al (2008) Mid-to Late Holocene climate change: an overview. Quat Sci Rev 27:1791–1828

Wigley TML, Briffa KR, Jones PD (1984) On the average of correlated time series, with applications in dendroclimatology and hydrometeorology. J Clim Appl Meteorol 23:201–213

Wilson RJS et al (2016) Last millennium Northern Hemisphere summer temperatures from tree rings. Part I: the long term context. Quat Sci Rev 134:1–18

Xoplaki E, González-Rouco JF, Gyalistras D, Luterbacher J, Rickli R, Wanner H (2003) Interannual summer air temperature variability over Greece and its connection to the large-scale atmospheric circulation and Mediterranean SSTs 1950–1999. Clim Dyn 20:537–554

Xoplaki E, Fleitmann D, Izdebski A, Luterbacher J, Wagner S, Zorita E, Telelis I, Toreti A (2016) The Medieval Climate Anomaly and Byzantium: a review of evidence on climatic fluctuations, economic performance and societal change. Quat Sci Rev 136:229–252

Xoplaki E et al (2018) Climate and societal resilience in the Eastern Mediterranean during the last millennium. Hum Ecol 46:363–379

Zanchettin D, Rubino A, Matei D, Bothe O, Jungclaus JH (2013) Multi-decadal-to-centennial SST variability in the MPI-ESM simulation ensemble for the last millennium. Clim Dyn 40:1301–1318